Nuclear Medicine and Biology 90–91 (2020) 98–103

Contents lists available at ScienceDirect

Nuclear Medicine and Biology

journal homepage: www.elsevier.com/locate/nucmedbio

Brown adipose tissue imaging using the TSPO tracer [^{18}F]fluoromethyl-PBR28-d_2: A comparison with [^{18}F]FDG

Chiwoo Oh [a], In Ho Song [b], Wooseung Lee [a], Miyeon Jeon [a], Jinyeong Choi [a], Seungki Baek [a], Byung Chul Lee [b,c,*], Sang Eun Kim [b,c,d], Hyung-Jun Im [a,d,**]

[a] Department of Applied Bioengineering, Graduate School of Convergence Science and Technology, Seoul National University, Seoul 08826, Republic of Korea
[b] Department of Nuclear Medicine, Seoul National University Bundang Hospital, Seoul National University College of Medicine, Seongnam 13620, Republic of Korea
[c] Center for Nanomolecular Imaging and Innovative Drug Development, Advanced Institutes of Convergence Technology, Suwon 16229, Republic of Korea
[d] Department of Molecular Medicine and Biopharmaceutical Sciences, Graduate School of Convergence Science and Technology, Seoul National University, Seoul 08826, Republic of Korea

ARTICLE INFO

Article history:
Received 10 May 2020
Received in revised form 2 September 2020
Accepted 17 October 2020

Keywords:
Brown adipose tissue
Translocator protein
Positron emission tomography

ABSTRACT

Introduction: Currently, the reference method of brown adipose tissue (BAT) imaging is ^{18}F-fluorodeoxyglucose positron emission tomography ([^{18}F]FDG PET). BAT imaging by [^{18}F]FDG PET requires additional stimulation process, which is inconvenient and hard to be standardized. The translocator protein 18 kDa (TSPO) PET has been found to be effective for visualization of BAT. Herein, we evaluated the feasibility of [^{18}F]fluoromethyl-PBR28-d_2 ([^{18}F]fmPBR28-d_2), a TSPO PET tracer, for interscapular BAT imaging in comparison with [^{18}F]FDG PET.
Methods: C57BL/6 mice were used for the [^{18}F]fmPBR28-d_2 and [^{18}F]FDG PET imaging. [^{18}F]fmPBR28-d_2 PET was performed in the thermoneutral condition (n = 5) and after cold exposure (4 °C for 4 h) on the next day using the same mice. [^{18}F]FDG PET was performed in the thermoneutral and cold exposure conditions with the same method with [^{18}F]fmPBR28-d_2 PET. Ex vivo biodistribution study of [^{18}F]fmPBR28-d_2 was performed in ten C57BL/6 mice (5: thermoneutral, 5: cold exposure). TSPO immunohistochemistry was done in interscapular BAT.
Results: The [^{18}F]fmPBR28-d_2 PET images showed prominent interscapular BAT uptakes under both thermoneutral and cold exposure conditions. While, the BAT uptake was significantly higher under the cold exposure condition than the thermoneutral condition (12.83 ± 5.06 vs. 22.50 ± 6.03, $P = 0.007$). Also, [^{18}F]FDG PET imaging showed higher BAT uptake under the cold exposure condition than thermoneutral condition (8.40 ± 0.63 vs. 21.41 ± 4.03, $P = 0.001$). The interscapular BAT to background (thigh muscle) ratio was higher in [^{18}F]fmPBR28-d_2 PET than [^{18}F]FDG PET under both thermoneutral and cold exposure conditions. Ex vivo biodistribution study using [^{18}F]fmPBR28-d_2 also showed higher BAT uptake under cold exposure than the thermoneutral condition (8.86 ± 1.74 vs.16.93 ± 4.74, $P = 0.036$). Also, IHC demonstrated that TSPO expression was significantly increased in the cold exposure group.
Conclusions: [^{18}F]FmPBR28-d_2 PET demonstrated prominent interscapular BAT uptakes regardless of additional stimulation, and showed a higher BAT to background ratio than [^{18}F]FDG PET. Also, we found that [^{18}F]fmPBR28-d_2 PET uptake and TSPO expression of BAT increased under cold exposure condition. Further works are warranted to assess the clinical significance of TSPO PET uptake in BAT.

1. Introduction

Brown adipose tissue (BAT) is a subtype of adipose tissue that characterized by a dense vasculature, sympathetic innervation, high mitochondria contents, and small lipid droplets [1]. White adipose tissue (WAT) is a storage site for excess energy mainly in the form of triglycerides, on the other hand, BAT is specialized for energy expenditure by non-shivering thermogenesis. Also, the activity of BAT was found to be lower in subjects with high body mass index (BMI), also in patients with type 2 diabetes compared to normal subjects [2,3]. Thus, BAT is emerging as a promising therapeutic target of obesity and metabolic disease. In particular, BAT transplantation improved hyperglycemia and obesity in multiple studies using rodent models of obesity and diabetes mellitus (DM) [4–6]. Also, the browning agents, which can modulate the phenotype of white adipocyte to brown adipocyte like cell (beige cell), demonstrated the effects on improving metabolic diseases [7–10].

For the successful development of BAT targeted obesity medicine, in vivo assessment of BAT is important because it is helpful for the selection of patient, prediction, and monitoring of the response to the medicine. Currently, the most commonly used BAT imaging method is ^{18}F-

* Correspondence to: B. C. Lee, Department of Nuclear Medicine, Seoul National University Bundang Hospital, Republic of Korea.
** Correspondence to: H.-J. Im, Department of Transdisciplinary Studies, Graduate School of Convergence Science and Technology, Seoul National University, Republic of Korea.

URL's: URL: http://tmtl.snu.ac.kr (B.C. Lee), iiihjjj@gmail.com iiihjjj@snu.ac.kr (H.-J. Im).

https://doi.org/10.1016/j.nucmedbio.2020.10.001
0969-8051/

fluorodeoxyglucose positron emission tomography ([^{18}F]FDG PET) [11]. However, BAT is detected in [^{18}F]FDG PET only about 3 to 8% of subjects if there is no activation process, although BAT can be found in 95% of subjects with activation process [3,12]. BAT activation can be done by cold exposure or administration of beta-3 adrenergic receptor agonist [13,14], however, the methods are inconvenient to the subjects and hard to be standardized [11]. Recently, the translocator protein 18 kDa (TSPO) targeting PET agents have been applied for BAT imaging because TSPO is expressed in the outer membrane of mitochondria, which is abundant in BAT. Ran et al. showed the BAT imaging capacity of [^{11}C] PBR28 in the human subject [15]. Also, Yang et al. reported that co-injection of disulfiram and $^{64}CuCl_2$ could be used to image TSPO in BAT [16]. Furthermore, it is reported that [^{18}F]DPA-714 PET can detect BAT, and the uptake was increased after BAT activation by CL 316,243 and cold exposure [17]. However, the imaging property of TSPO PET has not been compared with [^{18}F]FDG PET since now, the current method of choice for imaging BAT.

Herein, we investigated the BAT imaging ability of ^{18}F-labeled TSPO PET tracer, deuterium-substituted [^{18}F]fluoromethyl-PBR28 ([^{18}F] fmPBR28-d_2), and compared the imaging characteristics of [^{18}F] fmPBR28-d_2 PET with [^{18}F]FDG PET under thermoneutral and cold exposure conditions.

2. Methods

2.1. Radiochemistry

All reagents and solvent were purchased from Merck (Seoul, Republic of Korea) and used without further purification, unless otherwise specified. ^{18}F-Fluoride was produced by ^{18}O(p, n)^{18}F reaction through proton irradiation using a KOTRON-13 cyclotron at the Seoul National University Bundang Hospital (SNUH). [^{18}F]FDG was synthesized using a commercially available system (FASTlab platform, GE Healthcare) at SNUH facility and showed the permissible radiochemical purity (>98%) for patient use. The preparing TSPO radiotracer, [^{18}F]fmPBR28-d_2, needs two steps from dibromomethane-d_2. The radioactive intermediate ([^{18}F]fluoromethyl bromide-d_2) was prepared by the displacement of [^{18}F]fluoride, followed by the *O*-alkylation of desmethyl-PBR28 described previously [18,19].

2.2. [^{18}F]FmPBR28-d_2 PET imaging

All animal experimental protocols were approved by the Institutional Animal Care and Use Committee of Seoul National University. All mice were housed in specific pathogen free (SPF) facility. The five 8-week-old C57BL/6 female mice (OrientBio Inc., Seongnam, Korea) were used for TSPO PET imaging. [^{18}F]fmPBR28-d_2, a TSPO PET tracer, was injected into the mice intravenously (14.8 MBq in 200 μl saline per mouse). The mice were kept in the thermoneutral condition for 30 min after the injection. Before the scans, the mice were anesthetized with 2% isoflurane. Dynamic PET images for 60 min showed that the BAT uptake of [^{18}F]fmPBR28-d_2 was reached to the peak at 20 min after the injection and the uptake was steady until 60 min after the injection (Fig. S1). Thus, PET static images for 20 min were acquired after 30 min from intravenous injection using a NanoScan® PET/CT (Mediso Ltd., Budapest, Hungary). The next day, the same five mice were kept in the cold exposure condition at 4 °C for 4 h. After cold exposure, [^{18}F]fmPBR28-d_2 containing the same dose above was intravenously injected into the mice. The mice were kept in the cold exposure condition for 30 min. The PET static images of cold exposure condition were acquired by using the same methods.

2.3. [^{18}F]FDG PET imaging

The different five 8-week-old C57BL/6 female mice were used for [^{18}F]FDG PET imaging. The mice were fasted at least 8 h before [^{18}F]FDG PET imaging. [^{18}F]FDG was injected to the mice intravenously (1.11 MBq in 200 μl saline per mouse). The mice were kept in the thermoneutral condition for 1 h after injection. Before the scans, the mice were anesthetized with 2% isoflurane. The PET static images were acquired for 10 min using GENISYS4®, small animal PET scanner, (Sofie Biosciences, Culver City, USA). The next day, the same five mice were kept in the cold exposure condition at 4 °C for 4 h. After cold exposure, [^{18}F]FDG containing the same dose above was intravenously injected into the mice. The mice were kept in the cold exposure condition for 1 h. The PET static images were acquired by using the same methods.

2.4. Quantitative analysis using [^{18}F]fmPBR28-d_2 PET and [^{18}F]FDG PET imaging

Image visualization and volume of interest (VOI) analysis were performed by using MIM Encore® (MIM Software Inc., Cleveland, USA). The [^{18}F]fmPBR28-d_2 and [^{18}F]FDG uptakes of organs were quantified as the percentage of the injected dose per tissue weight (%ID/g) and standard uptake value (SUV). SUV was calculated by the formula (tissue radioactivity concentration)/[(injected dose)/(bodyweight)] using MIM Encore® software. VOI is measured for in vivo biodistribution and comparing the uptake between [^{18}F]fmPBR28-d_2 and [^{18}F]FDG. VOI for BAT was drawn on the interscapular region using fixed absolute threshold method (threshold: SUV 1.5) [12], and a sphere VOI with a diameter of 2.5 mm was drawn on the lateral side of left femur region and right liver lobe for the quantification of thigh muscle and liver uptake.

2.5. Ex vivo biodistribution

Ex vivo biodistribution study was performed in ten female 8-week-old C57BL/6 mice. The ten mice were divided into two groups: thermoneutral conditions and cold exposure conditions. The former group was kept in thermoneutral conditions at 25 °C. The latter group was kept in cold exposure condition at 4 °C for 4 h before an experiment. [^{18}F]fmPBR28-d_2 were injected intravenously (7.4 MBq in 200 μl per mice). The mice were sacrificed by asphyxia using carbon dioxide after 30 min of injection of [^{18}F]fmPBR28-d_2. The organs to be quantified were extracted from sacrificed mice. Extracted organs were blood, brain, heart, lung, kidney, adrenal gland, BAT, liver, stomach, muscle, intestine, and WAT. The extracted organs were weighed and radioactivity of ^{18}F was measured using an automatic gamma counter (1480 Wizard, Wallac, Turku, Finland). The %ID/g of organs was calculated using the weight of the tissue and the converting factor of the gamma counter.

2.6. Immunohistochemistry (IHC) and quantification

The organ tissues with 4% paraformaldehyde were embedded in paraffin. The paraffin was cut in 4 μm thick sections. The slices were placed in xylene twice for 3 min to remove the paraffin. In order to remove xylene, 100, 95, 90, 80, and 70% ethanol were treated for 3 min in regular sequence. The slices were placed in distilled water for 3 min then. After washing, 0.5% hydrogen peroxide in methanol was treated for 30 min. The slices fixed with the slice chamber were placed in 0.1% trypsin in phosphate buffer saline (PBS) and incubated with 20 min for antigen retrieval. After antigen retrieval, the 0.5% tritron™ X-100 (Sigma-Aldrich, St. Louis, MO) was treated for 3 min at 25 °C. The slices with 10% fetal bovine serum in PBS were incubated with 1 h for blocking unspecific binding. The primary antibody (1/250; EPR5384, Abcam, Cambridge, UK) was treated to stain TSPO of samples and overnight. After washing with PBS, the stained slices were incubated with Alexa Fluor® 488 (1/250; Abcam, Cambridge, UK) in the dark condition at 25 °C. We used SlowFade™ (S36938, Invitrogen, Grand Island, USA) to counterstain and mounting. In uncoupling protein 1 (UCP1) IHC, the primary antibody (1/4000; EPR20381, Abcam, Cambridge, UK) was treated to stain UCP1 of samples and Alexa Fluor® 555 (3 μg/ml; Abcam, Cambridge,

UK) was used for the secondary antibody. 4′,6-Diamidino-2-phenylindole (DAPI) was used for nuclear staining. The fluorescence images were acquired A1 Rsi confocal scanning microscope (Nikon, Tokyo, Japan) and obtained at 400× or 1200× magnification.

TSPO expression was quantified using fluorescence intensity. The imageJ was used to measure fluorescence intensity. The thresholding tool that is one of the imageJ function set the index what showed TSPO expression. In threshold menu, dark background and intermodes were chosen for fluorescence and threshold methods. Before analyzing staining signals the parameters were chosen to be measured. The selected parameters or options were means, standard deviation, gray level measurements, and limit to a threshold [20].

2.7. Statistical methods

The statistics of in-vivo imaging and TSPO expression were performed using GraphPad Prism's (GraphPad Software, CA, USA) statistical analysis. [^{18}F]FDG and [^{18}F]fmPBR28-d_2 uptakes were compared using the paired t-test between thermoneutral and cold conditions. Mann-Whitney tests were used to compare the TBRs of the scans, ex vivo biodistribution between cold and thermoneutral groups. Differences with $P < 0.05$ were considered significant.

3. Results

3.1. BAT imaging using [^{18}F]fmPBR28-d_2 in comparison with [^{18}F]FDG

[^{18}F]FmPBR28-d_2 PET imaging was performed under thermoneutral condition ($n = 5$). The next day, [^{18}F]fmPBR28-d_2 PET imaging was done in the same mice after 4 h of cold exposure. The [^{18}F]fmPBR28-d_2 PET images of all mice showed prominent BAT uptakes at the interscapular area under both thermoneutral and cold exposure conditions. Higher BAT uptake was noted under cold exposure than thermoneutral condition (Fig. 1A–B). Also, [^{18}F]FDG PET imaging was performed in five C57BL/6 mice under the thermoneutral condition and cold exposure condition at the next day. [^{18}F]FDG uptake in interscapular BAT was seen but not prominent under thermoneutral condition however the uptake was significantly enhanced under cold exposure condition (Fig. 1C–D). Quantified BAT uptake was increased in all mice in both [^{18}F]PBR28 (12.83 ± 5.06%ID/g vs. 22.50 ± 6.03% ID/g, $P = 0.007$, Fig. 2A) and [^{18}F]FDG PET groups (8.40 ± 0.63%ID/g vs. 21.41 ± 4.03%ID/g, $P = 0.001$, Fig. 2B). However, BAT to thigh muscle ratio was higher in [^{18}F]fmPBR28-d_2 group than [^{18}F]FDG PET group under both thermoneutral ([^{18}F]fmPBR28-d_2 vs. [^{18}F]FDG, 10.25 ± 2.89 vs. 4.44 ± 0.52, $P = 0.008$, Fig. 2C) and cold exposure condition ([^{18}F]fmPBR28-d_2 vs. [^{18}F]FDG, 14.31 ± 3.83 vs. 6.42 ± 1.39, $P = 0.008$, Fig. 2D). Also, BAT to liver ratio was higher in [^{18}F]fmPBR28-d_2 group than [^{18}F]FDG PET group under both thermoneutral ([^{18}F]fmPBR28-d_2 vs. [^{18}F]FDG, 5.88 ± 1.38 vs. 3.00 ± 0.64, $P = 0.008$, Fig. 2E) and cold exposure condition ([^{18}F]fmPBR28-d_2 vs. [^{18}F]FDG, 12.20 ± 2.19 vs. 9.16 ± 1.46, $P = 0.032$, Fig. 2F). [^{18}F]fmPBR28-d_2 uptake in trunk muscle was significantly lower than [^{18}F]FDG uptake in both cold exposure and thermoneutral conditions, which could be an advantage of [^{18}F]fmPBR28-d_2 PET over [^{18}F]FDG PET to evaluate BAT (Fig. S2). The BAT uptakes between thermoneutral and cold exposure conditions showed a trend of positive correlation, however it was not statistically significant both in [^{18}F]fmPBR28-d_2 PET ($R^2 = 0.536$, $P = 0.165$) and [^{18}F]FDG PET ($R^2 = 0.358$, $P = 0.286$) (Fig. S3).

3.2. Ex vivo biodistribution of [^{18}F]fmPBR28-d_2

Ex vivo biodistribution study at 30 min after the injection of [^{18}F]fmPBR28-d_2 was corroborated with the finding of the [^{18}F]fmPBR28-d_2 PET study. The %ID/g of brain, heart, lung, kidney, adrenal gland, and BAT were significantly higher under the cold exposure group than those under the thermoneutral group. However, the uptakes of blood, liver, stomach, muscle, femur, intestine, and WAT were not significantly different between the two groups (Fig. 3, Table 1).

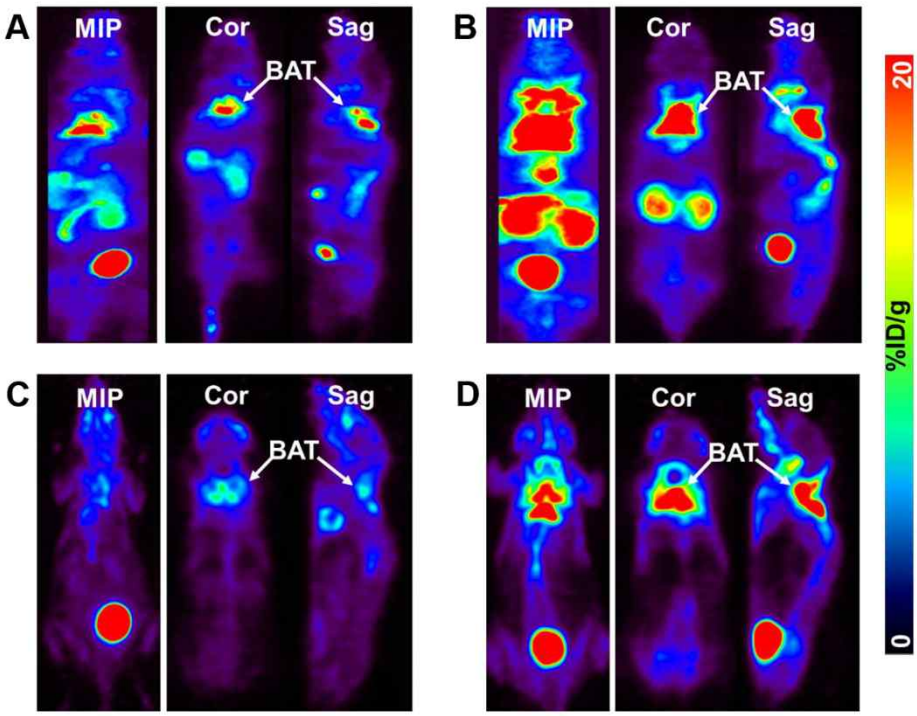

Fig. 1. In vivo BAT imaging using [^{18}F]fmPBR28-d_2 in comparison with [^{18}F]FDG. The PET images were acquired using tracers, [^{18}F]fmPBR28-d_2 (A, B) and [^{18}F]FDG (C, D) and displayed in MIP (left), coronal (middle) and sagittal section (right). The prominent BAT uptakes were shown in the images of [^{18}F]fmPBR28-d_2 under thermoneutral condition (A). On the other hand, BAT uptakes was not prominent under thermoneutral condition using [^{18}F]FDG (C). Both [^{18}F]fmPBR28-d_2 and [^{18}F]FDG PET images showed prominent BAT uptakes in the interscapular region under cold exposure condition (B, D). BAT: brown adipose tissue, MIP: maximum intensity projection, Cor: coronal, Sag: sagittal.

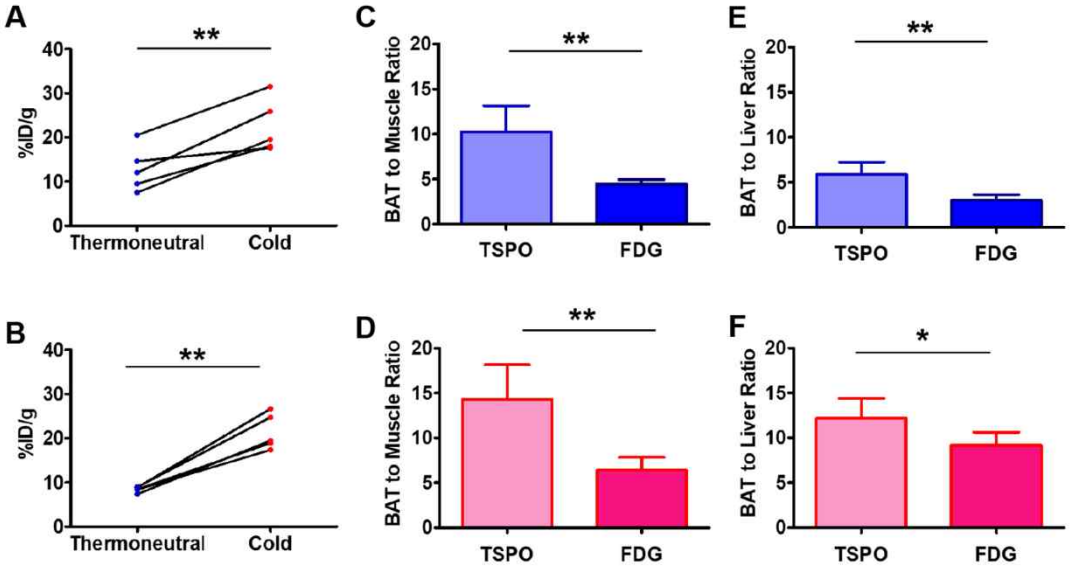

Fig. 2. The graphs of quantified BAT uptakes in [^{18}F]fmPBR28-d_2 PET and [^{18}F]FDG PET. A, B. The graphs showed higher BAT uptakes of [^{18}F]fmPBR28-d_2 (n = 5) (A) and [^{18}F]FDG (n = 5) (B) under the cold exposure condition than in the thermoneutral condition. BAT to thigh muscle ratios (C, D) and BAT to liver ratios (E, F) were compared. [^{18}F]fmPBR28-d_2 PET showed higher BAT to normal organ ratios both under thermoneutral condition (C, E) and cold exposure condition (D, F) than [^{18}F]FDG PET. BAT: brown adipose tissue, TSPO: [^{18}F]fmPBR28-d_2 PET, FDG: [^{18}F]FDG PET, *: $P < 0.05$, **: $P < 0.01$.

3.3. IHC analysis of BAT during cold exposure

UCP1 IHC revealed that UCP1 expression in BAT was higher in cold exposure group compared to the thermoneutral group (Fig. S4). In IHC analysis using anti-TSPO antibody, the fluorescence intensities of TSPO in BAT was brighter in the cold exposure group than the thermoneutral group (Fig. 4A). Also, the quantified TSPO expression in BAT was significantly higher under the cold exposure group (n = 5) than the thermoneutral group (n = 5) (Fig. 4B).

4. Discussion

In this study, we utilized [^{18}F]fmPBR28-d_2 for BAT imaging in normal mice under both thermoneutral and cold exposure conditions. We found that there was significant [^{18}F]fmPBR28-d_2 uptake in the BAT under both conditions, and the uptake was higher under cold exposure than thermoneutral condition. When the BAT uptake was compared between [^{18}F]FDG PET and [^{18}F]fmPBR28-d_2 PET, BAT to background ratio was higher in [^{18}F]fmPBR28-d_2 PET than [^{18}F]FDG PET under both conditions.

Currently, [^{18}F]FDG PET is the reference standard imaging method for BAT, while other various imaging methods are under investigation including single photon emission computed tomography (SPECT), magnetic resonance imaging (MRI) and computed tomography (CT) [11]. Chemical-shift Dixon MRI has been found to detect BAT by measuring the fat fraction and R2* of tissue, since BAT has a lower amount of lipid and higher R2* value than WAT [21]. However, the MR signals are not specific for BAT and hard to be separated between BAT and WAT [11,22]. Meanwhile, Branca et al. reported that Xenon enhanced CT (XECT) could accurately quantify BAT, which showed a good agreement with [^{18}F]FDG PET. However, XECT requires an additional stimulation process for the detection of BAT and both scans (with and without stimulation) for the quantification of BAT [23]. ^{99m}Tc-methoxyisobutylisonitrile (MIBI) SPECT has been suggested to be

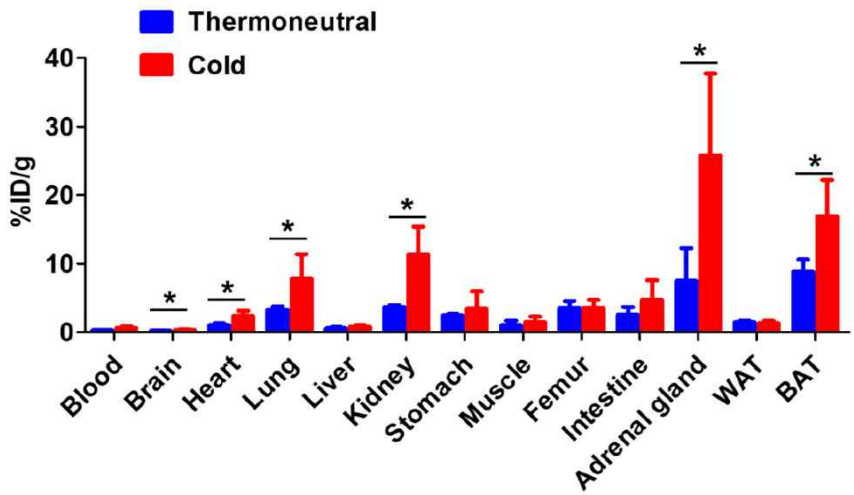

Fig. 3. Ex vivo biodistribution of [^{18}F]fmPBR28-d_2 between thermoneutral condition (n = 5) and cold exposure condition (n = 5). The organs were extracted from sacrificed mice. The quantified BAT uptakes of two groups were compared by independent sample t-test. The graph showed that radiotracer uptakes of brain, heart, lung, kidney, adrenal gland and BAT were significantly increased under cold exposure condition. On the other hand, the radiotracer uptakes of blood, liver, stomach, muscle, femur, intestine, and WAT did not show significant differences between thermoneutral condition and cold exposure condition. WAT: white adipose tissue, BAT: brown adipose tissue, *: $P < 0.05$.

Table 1
Ex vivo biodistribution of [^{18}F]fmPBR28-d_2.

Organs	Thermoneutral (n = 5) (%ID/g)		Cold exposure (n = 5) (%ID/g)		*P* value
	Average	SD	Average	SD	
Blood	0.30	0.03	0.61	0.21	0.059
Brain	0.21	0.03	0.34	0.09	0.036*
Heart	1.03	0.27	2.36	0.68	0.012*
Lung	3.30	0.46	7.86	3.15	0.021*
Liver	0.56	0.18	0.80	0.23	0.141
Kidney	5.09	0.38	11.34	3.65	0.012*
Stomach	2.46	0.19	3.45	2.24	1.000
Muscle	1.02	0.67	1.47	0.73	0.207
Femur	3.60	0.95	3.58	1.03	0.834
Intestine	2.58	1.11	4.77	2.51	0.293
Adrenal gland	7.48	4.75	25.74	10.74	0.036*
WAT	1.48	0.20	1.31	0.29	0.207
BAT	8.86	1.74	16.93	4.74	0.036*

WAT: white adipose tissue, BAT: brown adipose tissue, SD: standard deviation.
Mann-Whitney tests was performed for statistical analysis.
* $P < 0.05$.

used for BAT imaging [24,25]. Although the precise mechanism of ^{99m}Tc-MIBI uptake to BAT has not been elucidated, it is considered that the high mitochondrial contents of BAT are the main reason since ^{99m}Tc-MIBI is localized primarily in mitochondria of the cells [26]. Recently, TSPO is getting attention for a target of BAT imaging. Several studies showed that various TSPO PET agents could visualize BAT. For example, Hartimath et al. reported that TSPO can be used for imaging adipocyte browning after beta3 adrenergic agonist administration [27]. However, the effect of acute cold exposure in comparison with [^{18}F]FDG PET has not been reported [15–17,27]. In our study, we found that [^{18}F]fmPBR28-d_2 PET has a higher BAT to background ratio under both thermoneutral and cold exposure conditions than [^{18}F]FDG PET, which suggests an advantage of TSPO PET over [^{18}F]FDG PET for BAT imaging. Also, we found that the BAT uptake of [^{18}F]fmPBR28-d_2 was enhanced under cold exposure condition.

TSPO has various functions including transportation of cholesterol, regulation of reactive oxygen species (ROS), and production of cellular energy [28]. Although the roles of TSPO in BAT has not been well evaluated, Thompson et al. reported that TSPO expression of BAT is reduced in the model of obesity suggesting potential roles of TSPO in energy expenditure of BAT. In the study, the authors also found that TSPO expression was not changed under cold exposure [29], which is in contrary to our finding. This discrepancy could be caused by different experiment settings. While mitochondrial extracts of BAT were used in the previous study [29], we utilized the in vivo PET imaging, ex vivo biodistribution study, and IHC of TSPO using anti-TSPO antibody. Among the previous TSPO PET studies, Wang et al. reported that [^{18}F]DPA-714 uptake was increased by cold exposure, which is in line with our finding [17]. This enhanced uptake of TSPO PET agents in BAT under cold exposure may lead to a hypothesis that TSPO has a role for non-shivering thermogenesis in BAT.

In the present study, interscapular BAT of mouse was explored as representative BAT in mouse. Interscapular BAT consists of classical brown adipocytes while inducible brite cells can be found in inguinal WAT. It has been found that brite fat in mouse inguinal area has a higher molecular similarity with human BAT than interscapular BAT [30]. However, we could not find any focal uptake in inguinal area in FDG and TSPO PET imaging in thermoneutral and cold exposure conditions. This was in accordance with previous reports using [^{18}F]FDG PET and [^{18}F]FEPPA agent [3,7]. Zhang et al. reported that FDG uptake in inguinal WAT region was not apparent even after 7 days of beta3 agonist treatment [7]. Also, Hartimath et al. reported that [^{18}F]FEPPA, TSPO PET agent, was not able to detect signal on day 1 after beta3 adrenergic agonist stimulation [3]. Thus, we speculate that the number of existing brite cells are not sufficient to be seen on in vivo imaging before chronic adrenergic stimulation.

Cold exposure has been known to modulate the metabolism of multiple organs including adrenal gland, skeletal muscle, adipose tissues, kidney and liver [31,32]. For example, cold exposure resulted in glycogen and lipid depletion in the liver and the adrenal gland [33], and modulates mitochondrial biogenesis in skeletal muscle and white adipose tissue [34]. Also in BAT, cold exposure facilitates fatty acid synthesis/oxidation [35], and alters the amino acids, nucleotide pathways, and metabolites involved in redox regulation [36]. Meanwhile, TSPO has been reported to have a role in metabolic changes in steroidogenic cells and BAT [29,37]. We found that multiple organs showed enhanced TSPO tracer uptake under cold exposure in ex vivo biodistribution study, which are the brain, heart, lung, kidney, adrenal gland, and BAT. These organs, except brain, are also known to have high expressions of TSPO [38]. In particular, the adrenal gland is the highest TSPO expressing organ and showed the most prominent enhancement of [^{18}F]fmPBR28-d_2 uptake (4.2 fold change) after the cold exposure in our study. Also, we found that low TSPO expressing organs such as bone, stomach showed no significant changes after the cold exposure. Taken together,

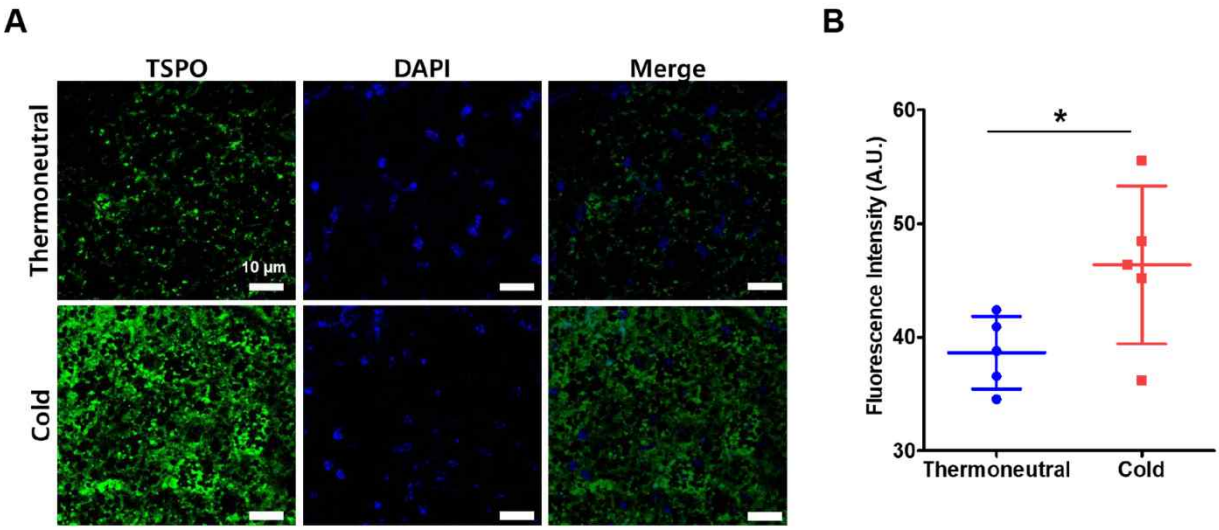

Fig. 4. TSPO IHC of BAT in thermoneutral and cold exposure groups. A. TSPO expression was enhanced after cold exposure in BAT. DAPI stains were similar between the groups. The TSPO fluorescence intensity of BAT was quantified and compared between thermoneutral (n = 5) and cold exposure groups (n = 5). Fluorescence intensity of TSPO expression was significantly higher in the cold exposure group than the thermoneutral group. TSPO: translocator protein, *: $P < 0.05$, DAPI: 4′,6-diamidino-2-phenylindole.

it is speculated that TSPO may have a dynamic role to modulate cold exposure induced metabolic changes in multiple organs with high TSPO expression including BAT and adrenal gland.

There are several limitations in this study. The [^{18}F]fmPBR28-d_2 and [^{18}F]FDG PET imaging were done in two different PET scanners. However, we used BAT to muscle ratio to compare the images to reduce the confounding factors which may be caused by using the different machines. Although we presented the advantage of [^{18}F]fmPBR28-d_2 PET over [^{18}F]FDG PET for BAT imaging, the clinical significance of [^{18}F]fmPBR28-d_2 uptake in BAT has not been evaluated. More specifically, [^{18}F]fmPBR28-d_2 uptake in BAT at thermoneutral condition was not associated with that at cold exposure condition. Therefore the clinical significance of [^{18}F]fmPBR28-d_2 uptake in BAT either at thermoneutral or cold exposure condition should be addressed in the further studies. It was hard to conclude if there was correlation of the tracer uptakes between cold and thermoneutral conditions, because of small number of animals. Also, mechanism study to reveal the role of enhanced TSPO uptake in BAT under cold exposure condition has not been performed in the present study. Further studies are warranted to evaluate the clinical significance of TSPO PET BAT imaging and the mechanism of enhanced TSPO uptake under cold exposure.

5. Conclusions

We found that [^{18}F]fmPBR28-d_2 PET was feasible for interscapular BAT imaging under both thermoneutral and cold exposure conditions in mice. [^{18}F]fmPBR28-d_2 PET showed higher BAT to background ratio under both conditions than [^{18}F]FDG PET. [^{18}F]FmPBR28-d_2 could be used as a BAT imaging agent which can be used without activation process. Further research on finding the clinical significance of BAT imaging using TSPO PET is warranted.

Acknowledgements

This work was supported by Research Resettlement Fund for the new faculty of Seoul National University. This study was supported by National Research Foundation of Korea (NRF) (NRF-2017R1D1A1B03035556, NRF-2019M2D2A1A01058210, and NRF-2020R1C1C1009000), the Ministry of Health and Welfare Korea (HI18C0886, and HI19C0339), Creative-Pioneering Researchers Program through Seoul National University (SNU) and the SNUBH Research Fund 13-2018-009.

Declaration of competing interest

No potential conflicts of interest relevant to this article exist.

Appendix A. Supplementary data

Supplementary data to this article can be found online at https://doi.org/10.1016/j.nucmedbio.2020.10.001.

References

[1] Betz MJ, Enerback S. Targeting thermogenesis in brown fat and muscle to treat obesity and metabolic disease. Nat Rev Endocrinol. 2018;14:77–87.
[2] Cypess AM, Lehman S, Williams G, et al. Identification and importance of brown adipose tissue in adult humans. N Engl J Med. 2009;360:1509–17.
[3] van Marken Lichtenbelt WD, Vanhommerig JW, Smulders NM, et al. Cold-activated brown adipose tissue in healthy men. N Engl J Med. 2009;360:1500–8.
[4] Min SY, Kady J, Nam M, et al. Human 'brite/beige' adipocytes develop from capillary networks, and their implantation improves metabolic homeostasis in mice. Nat Med. 2016;22:312–8.
[5] Gunawardana SC, Piston DW. Reversal of type 1 diabetes in mice by brown adipose tissue transplant. Diabetes. 2012;61:674–82.
[6] Liu X, Zheng Z, Zhu X, et al. Brown adipose tissue transplantation improves whole-body energy metabolism. Cell Res. 2013;23:851.
[7] Kaisanlahti A, Glumoff T. Browning of white fat: agents and implications for beige adipose tissue to type 2 diabetes. J Physiol Biochem. 2019;75:1–10.
[8] Beiroa D, Imbernon M, Gallego R, et al. GLP-1 agonism stimulates brown adipose tissue thermogenesis and browning through hypothalamic AMPK. Diabetes. 2014;63:3346–58.
[9] Qiang L, Wang L, Kon N, et al. Brown remodeling of white adipose tissue by SirT1-dependent deacetylation of Ppargamma. Cell. 2012;150:620–32.
[10] Ghorbani M, Himms-Hagen J. Appearance of brown adipocytes in white adipose tissue during CL 316,243-induced reversal of obesity and diabetes in Zucker fa/fa rats. Int J Obes Relat Metab Disord. 1997;21:465–75.
[11] Sampath SC, Sampath SC, Bredella MA, Cypess AM, Torriani M. Imaging of brown adipose tissue: state of the art. Radiology. 2016;280:4–19.
[12] Bauwens M, Wierts R, van Royen B, et al. Molecular imaging of brown adipose tissue in health and disease. Eur J Nucl Med Mol Imaging. 2014;41:776–91.
[13] Cypess Aaron M, Weiner Lauren S, Roberts-Toler C, et al. Activation of human brown adipose tissue by a β3-adrenergic receptor agonist. Cell Metab. 2015;21:33–8.
[14] Chen Kong Y, Cypess Aaron M, Laughlin Maren R, et al. Brown Adipose Reporting Criteria in Imaging STudies (BARCIST 1.0): recommendations for standardized FDG-PET/CT experiments in humans. Cell Metab. 2016;24:210–22.
[15] Ran C, Albrecht DS, Bredella MA, et al. PET imaging of human brown adipose tissue with the TSPO tracer [^{11}C]PBR28. Mol Imaging Biol. 2018;20:188–93.
[16] Yang J, Yang J, Wang L, Moore A, Liang SH, Ran C. Synthesis-free PET imaging of brown adipose tissue and TSPO via combination of disulfiram and (64)$CuCl_2$. Sci Rep. 2017;7:8298.
[17] Wang Y, Jacobson O, Niu G, Chen X. PET imaging of brown adipose tissue using fluorine 18-labeled TSPO ligand DPA-714. J Nucl Med. 2017;58:480.
[18] Moon BS, Jung JH, Park HS, et al. Preclinical comparison study between [^{18}F]fluoromethyl-PBR28 and its deuterated analog in a rat model of neuroinflammation. Bioorg Med Chem Lett. 2018;28:2925–9.
[19] Moon BS, Kim BS, Park C, et al. [^{18}F]Fluoromethyl-PBR28 as a potential radiotracer for TSPO: preclinical comparison with [^{11}C]PBR28 in a rat model of neuroinflammation. Bioconjug Chem. 2014;25:442–50.
[20] Jensen EC. Quantitative analysis of histological staining and fluorescence using ImageJ. Anat Rec (Hoboken). 2013;296:378–81.
[21] Hu HH, Perkins TG, Chia JM, Gilsanz V. Characterization of human brown adipose tissue by chemical-shift water-fat MRI. AJR Am J Roentgenol. 2013;200:177–83.
[22] Deng J, Neff LM, Rubert NC, et al. MRI characterization of brown adipose tissue under thermal challenges in normal weight, overweight, and obese young men. J Magn Reson Imaging. 2018;47:936–47.
[23] Branca RT, McCallister A, Yuan H, et al. Accurate quantification of brown adipose tissue mass by xenon-enhanced computed tomography. Proc Natl Acad Sci U S A. 2018;115:174–9.
[24] Cypess AM, Doyle AN, Sass CA, et al. Quantification of human and rodent brown adipose tissue function using 99mTc-methoxyisobutylisonitrile SPECT/CT and ^{18}F-FDG PET/CT. J Nucl Med. 2013;54:1896–901.
[25] Goetze S, Lavely WC, Ziessman HA, Wahl RL. Visualization of brown adipose tissue with 99mTc-methoxyisobutylisonitrile on SPECT/CT. J Nucl Med. 2008;49:752–6.
[26] Arbab AS, Koizumi K, Toyama K, Arai T, Araki T. Technetium-99m-tetrofosmin, technetium-99m-MIBI and thallium-201 uptake in rat myocardial cells. J Nucl Med. 1998;39:266–71.
[27] Hartimath SV, Khanapur S, Boominathan R, et al. Imaging adipose tissue browning using the TSPO-18 kDa tracer [^{18}F]FEPPA. Mol Metab. 2019;25:154–8.
[28] Batarseh A, Papadopoulos V. Regulation of translocator protein 18 kDa (TSPO) expression in health and disease states. Mol Cell Endocrinol. 2010;327:1–12.
[29] Thompson MM, Manning HC, Ellacott KLJ. Translocator protein 18 kDa (TSPO) is regulated in white and brown adipose tissue by obesity. PloS One. 2013;8:e79980.
[30] Sharp LZ, Shinoda K, Ohno H, et al. Human BAT possesses molecular signatures that resemble beige/brite cells. PloS One. 2012;7:e49452.
[31] Trzcionka M, Withers KW, Klingenspor M, Jastroch M. The effects of fasting and cold exposure on metabolic rate and mitochondrial proton leak in liver and skeletal muscle of an amphibian, the cane toad Bufo marinus. J Exp Biol. 2008;211:1911–8.
[32] Guernsey DL, Stevens ED. The cell membrane sodium pump as a mechanism for increasing thermogenesis during cold acclimation in rats. Science. 1977;196:908–10.
[33] Ferreira M, de Abreu LC, Valenti VE, Meneghini A, Murad N, Ferreira C. Electric countershock and cold stress effects on liver and adrenal gland. Clinics (Sao Paulo, Brazil). 2010;65:291–6.
[34] Chung N, Park J, Lim K. The effects of exercise and cold exposure on mitochondrial biogenesis in skeletal muscle and white adipose tissue. J Exerc Nutr Biochem. 2017;21:39–47.
[35] Yu XX, Lewin DA, Forrest W, Adams SH. Cold elicits the simultaneous induction of fatty acid synthesis and beta-oxidation in murine brown adipose tissue: prediction from differential gene expression and confirmation in vivo. FASEB J. 2002;16:155–68.
[36] Lu X, Solmonson A, Lodi A, et al. The early metabolomic response of adipose tissue during acute cold exposure in mice. Sci Rep. 2017;7:3455.
[37] Tu LN, Zhao AH, Hussein M, Stocco DM, Selvaraj V. Translocator protein (TSPO) affects mitochondrial fatty acid oxidation in steroidogenic cells. Endocrinology. 2016;157:1110–21.
[38] Banati RB, Middleton RJ, Chan R, et al. Positron emission tomography and functional characterization of a complete PBR/TSPO knockout. Nat Commun. 2014;5:5452.